Chapter 4
Diffusion of Chemically Reacting Fluids through Nonlinear Elastic Solids and 1D Stabilized Solutions

Richard Hall, H. Gajendran, and A. Masud

Abstract This paper summarizes a 1D adaptation (Hall et al., Math Mech Solids, 2014) of the reactive fluid–solid mixture theory of Hall and Rajagopal (Math Mech Solids 17(2):131–164, 2012), which considers an anisotropic viscous fluid diffusing and chemically reacting with an anisotropic elastic solid. The present implementation introduces a stabilized mixed finite element method for advection–diffusion–reaction phenomena, which is applied to 1D isothermal problems involving Fickian diffusion, oxidation of PMR-15 polyimide resin, and slurry infiltration. The energy and entropy production relations are captured via a Lagrange multiplier that results from imposing the constraint of maximum rate of entropy production, reducing the primary PDEs to the balance equations of mass and linear momentum for the fluid and the solid, together with an equation for the Lagrange multiplier. The Fickian diffusion application considers a hyperbolic first-order system with a boundary discontinuity and stable approach to the usual parabolic model. Results of the oxidation modeling of Tandon et al. (Polym Degrad Stab 91(8):1861–1869, 2006) are recovered by employing the reaction kinetics model and properties assumed there, while providing in addition the individual constituent kinematic and kinetic behaviors, thus adding rich interpretive detail in comparison to the original treatment (Tandon et al., Polym Degrad Stab 91 (8):1861–1869, 2006); two adjustable parameters describing coupled chemomechanical and purely chemical dissipation are added. The slurry infiltration application simulates the imposed mass deposition process and consequent effects on the kinematic and kinetic behaviors of the constituents.

Keywords Mixture • Reaction • Dissipation • Stabilized • Slurry

4.1 General Mixture Theory

The equations of mass and linear momentum balance for the diffusion of a chemically reacting fluid through a finitely deforming thermoelastic solid are given as follows [1]:

$$\text{Balance of mass}: \quad \frac{D^{\alpha}\rho^{\alpha}}{dt} + \rho^{\alpha}\text{div}\boldsymbol{\nu}^{\alpha} = \frac{\partial \rho^{\alpha}}{\partial t} + \text{div}(\rho^{\alpha}\boldsymbol{\nu}^{\alpha}) = m^{\alpha} \tag{4.1}$$

$$\text{Balance of linear momentum}: \quad \rho^{\alpha}\frac{D^{\alpha}\boldsymbol{\nu}^{\alpha}}{dt} = \text{div}(\mathbf{T}^{\alpha})^{T} + \rho^{\alpha}\mathbf{b} + \mathbf{I}^{\alpha} \tag{4.2}$$

where, ρ^{α} is the mass concentration and m^{α} is the rate of mass transferred by chemical reaction, to constituent α, per unit mixture volume; $\boldsymbol{\nu}^{\alpha}$ is the velocity of constituent α and $\mathbf{T}^{\alpha}$ is its partial Cauchy stress, while $\mathbf{I}^{\alpha}$ and $\mathbf{b}$ are the interactive force per unit mixture volume on constituent α and the body force per unit mass.

R. Hall (✉)
Materials and Manufacturing Directorate, Air Force Research Laboratory, AFRL/RXBC Bldg 654, 2941, WPAFB, Hobson Way, OH 45433-7750, USA

H. Gajendran • A. Masud
Department of Civil and Environmental Engineering, University of Illinois at Urbana-Champaign, 205 North Mathews Ave., Urbana, IL 61801-2352, USA

H.J. Qi et al. (eds.), *Challenges in Mechanics of Time-Dependent Materials, Volume 2: Proceedings of the 2014 Annual Conference on Experimental and Applied Mechanics*, Conference Proceedings of the Society for Experimental Mechanics Series,
DOI 10.1007/978-3-319-06980-7_4,

The balance of energy and assumption of maximized rate of entropy production, together with Newton's third law, lead to the following relations for the partial stresses on the solid and fluid, $\mathbf{T}^s$ and $\mathbf{T}^f$; the interactive force $\mathbf{I}^f$ on the fluid, the constituent entropy η^α, and the rate of fluid mass conversion, m^f, all per unit mixture volume; and the heat flux $\boldsymbol{q}$, per unit mixture area:

$$\mathbf{I}^f = g^f \frac{\rho^s}{\rho} \nabla \rho^f - g^s \frac{\rho^f}{\rho} \nabla \rho^s - \nabla \left[\frac{\rho^s \rho^f}{\rho} \left(\psi^f - \psi^s \right) \right] - (\nabla \theta) \frac{\rho^s \rho^f}{\rho} \left(\eta^f - \eta^s \right) - m^f \left(\boldsymbol{\nu}^f - \boldsymbol{\nu}^s \right) - \mu \, \mathbf{A}^v \left(\boldsymbol{\nu}^f - \boldsymbol{\nu}^s \right) \tag{4.3}$$

$$\mathbf{T}^s = \rho \mathbf{F}^s \left(\frac{\partial \psi}{\partial \mathbf{F}^s} \right)^T - \rho^s \left(g^s + \frac{\rho^f}{\rho} \left(\psi^f - \psi^s \right) \right) \mathbf{I} \tag{4.4}$$

$$\mathbf{T}^f = -\rho^f \left(g^f + \frac{\rho^s}{\rho} \left(\psi^s - \psi^f \right) \right) \mathbf{I} + \mu \, \mathbf{A}^L \cdot \mathbf{D}^f \tag{4.5}$$

$$\eta^\alpha = -\frac{\partial \psi^\alpha}{\partial \theta} - \frac{\mu}{\rho} c_\theta^\alpha \dot{\theta} \tag{4.6}$$

$$\frac{\mathbf{q}}{\theta} = -\mu \, \boldsymbol{l} \, \nabla \theta + \frac{\rho^s \rho^f}{\rho} \left(\eta^f - \eta^s \right) \left(\boldsymbol{\nu}^f - \boldsymbol{\nu}^s \right) \tag{4.7}$$

$$m^f = \frac{1}{\mu c_{\mathrm{m}}} \left[-\left(g^f - g^s \right) - \frac{1}{2} \left(\boldsymbol{\nu}^f - \boldsymbol{\nu}^s \right) \cdot \left(\boldsymbol{\nu}^f - \boldsymbol{\nu}^s \right) \right] \tag{4.8}$$

where the chemical potential g^α of constituent α is defined through

$$g^\alpha \equiv \rho \frac{\partial \psi}{\partial \rho^\alpha} \tag{4.9}$$

ρ, ψ and θ are the mixture density, mixture Helmholtz energy and temperature; while ψ^α are the constituent Helmholtz energies; Material parameters ${c_\theta}^\alpha$ and c_{m} are respectively associated with the constituent entropies, and with mass transfer, while $\boldsymbol{l}$ is the mixture thermal conductivity tensor; $\mathbf{F}^s$ is the solid deformation gradient; $\mathbf{A}^v$ and $\mathbf{A}^L$ are drag and viscosity coefficient tensors and $\mathbf{D}^f$ is the fluid rate of deformation tensor.

The rate of mass transfer to the fluid, m^f, is determined in coordination with the orientation average of the rate of reaction tensor $\dot{\Gamma}$. Because of the presence of only two constituents, the mass balance provides that the rate of mass converted to the solid is the one lost from the fluid:

$$m^s = -m^f \tag{4.10}$$

In the diffusion-dominated approximation (diffusion of the reactants is far more rapid than the reaction), the operator $\dot{\Pi}\{\mathbf{n}, \mathbf{X}^s, t\}$ provides the directional solid mass conversion rate in the direction -$\boldsymbol{n}$, per unit mixture volume, such that:

$$m^s = \frac{1}{4\pi} \int_{\alpha=0}^{4\pi} \dot{\Pi}\{\mathbf{n}[\alpha], \mathbf{X}^s, t\} \, d\alpha \tag{4.11}$$

where, $\boldsymbol{n}$ is the outward unit normal, $\mathbf{X}^s$ is the reference coordinate of the solid, α is the solid angle, and a second-order representation is assumed for the operator $\dot{\Pi}\{\mathbf{n}, \mathbf{X}^s, t\}$

$$\dot{\Pi}\{\mathbf{n}, \mathbf{X}^s, t\} \approx \mathbf{n} \cdot \dot{\Gamma} \left[\mathbf{X}^s, t \right] \mathbf{n} \tag{4.12}$$

with the tensor

$$\Gamma\left[\mathbf{X}^s, t\right] = \int_0^t \dot{\Gamma}\left[\mathbf{X}^s, \overline{t}\right] d\overline{t} \tag{4.13}$$

thus, providing an anisotropic measure of the extent of reaction of the solid.

The Lagrange multiplier μ arises from the constraint of maximized rate of entropy production [1]. Because η^α and m^f depend on μ, a cubic equation in μ results. To obtain a single-valued relation for μ, the following approximations are made:

1. We assume that the attributes of the Helmholtz free energy functions of the constituents and the mixture can be represented in terms of suitably condensed forms, $\psi^s = \psi^f = \psi$, $\eta^s = \eta^f = \eta$.
2. Slow diffusion permits neglect of the squared relative kinetic energy terms $((\boldsymbol{\nu}^f - \boldsymbol{\nu}^s) \cdot (\boldsymbol{\nu}^f - \boldsymbol{\nu}^s))^2$, which are assumed also negligible relative to the drag force.
3. We assume that the reaction is near enough to equilibrium to neglect the squared difference in the chemical potentials of the constituents, and the product of the chemical potential difference with the relative kinetic energy.

The Lagrange multiplier is thus reduced to the following single-valued function:

$$\mu = \frac{1}{2} + \frac{\frac{1}{4}\dot{\Gamma}^0_{IJ}\Gamma^0_{KL}\Gamma^0_{MN}E^s_{OP}K^0_{IJKLMNOP}}{\left\{\begin{array}{l}\mathbf{D}^f \cdot \mathbf{A}^L \cdot \mathbf{D}^f + c_\theta \dot{\theta}^2 + \left(\boldsymbol{\nu}^f - \boldsymbol{\nu}^s\right) \cdot \mathbf{A}^{\boldsymbol{\nu}}\left(\boldsymbol{\nu}^f - \boldsymbol{\nu}^s\right) + \\ \dot{\Gamma}^0 \cdot \mathbf{A}^{0\Gamma} \cdot \dot{\Gamma}^0 + \nabla\theta \cdot \mathbf{l}\nabla\theta + \frac{1}{2}\dot{\Gamma}^0_{AB}\Gamma^0_{CD}\Gamma^0_{EF}E^s_{GH}K^0_{ABCDEFGH}\end{array}\right\}} \tag{4.14}$$

$\mathbf{E}^s$ is the Lagrangian solid strain measure and Γ is referred to material coordinates. The tensor $\boldsymbol{K^0}$ will have mostly zero-valued components. If reaction processes such as oxidation are considered, in which the reaction is several times faster in the fiber direction than the transverse directions thus promoting a unidirectional reaction assumption, and assuming transversely isotropic coupling to the strains, the term involving $\boldsymbol{K^0}$ reduces to the following expression, involving four independent constants:

$$\dot{\Gamma}^0_{IJ}\Gamma^0_{KL}\Gamma^0_{MN}E^s_{OP}K^0_{IJKLMNOP} = \dot{\Gamma}^0_{11}\left(\Gamma^0_{11}\right)^2\left[K^0_1 E^s{}_{11} + K^0_2(E^s{}_{22} + E^s{}_{33}) + K^0_3(E^s{}_{12} + E^s{}_{31}) + K^0_4 E^s{}_{23}\right] \tag{4.15}$$

In the present work, the influence of the energy and entropy production relations are retained through the presence of the Lagrange multiplier, which is obtained via invoking the constraint of maximized rate of entropy production. The equations explicitly retained are the constituent momentum balances and the mass balance equation, which can be considered most strongly enforced. In accordance with the present study being isothermal, the traditional heat capacity measures of the constituents are lost through the assumption above that the constituent entropy functions can be replaced by an overall entropy function. In general for anisothermal processes, the Helmholtz and entropy functions of each constituent would be retained. It is interesting to note, however, that the present system of equations incorporates the rate of temperature in combination with a non-traditional overall material property c_θ (the density average of the $c_\theta{}^\alpha$ properties), which may provide a simplified approach to accounting for a class of homogenized anisothermal effects. The present paper however considers only isothermal conditions.

We consider the following Helmholtz free energy function that corresponds to the 1-D representation of a transversely isotropic thermoelastic solid permeated by a chemically reacting Newtonian fluid.

$$\begin{aligned}\psi = {} & A^s + (B^s + c^s)\left(\theta - \theta^s\right) - \frac{c^s_1}{2}\left(\theta - \theta^s\right)^2 - c^s_2\theta\ln\left(\frac{\theta}{\theta^s}\right) + \frac{1}{\rho_T}\left\{\overline{R}\theta\rho^f + k^f_2\rho^f\right\} \\ & + \frac{\rho^s}{\rho}\frac{1}{\rho^s_T}\left\{\frac{1}{2}\lambda^s + \mu^s_T + \alpha^s + 2\left(\mu^s_L - \mu^s_T\right) + \frac{1}{2}\beta^s\right\}\left(E^s_{11}\right)^2 + \Lambda\end{aligned} \tag{4.16}$$

$$\Lambda = \int \frac{\mu}{2}\left\{\left(\Gamma^0_{11}\right)^2\overline{K}_1 E^s_{11} + 2\dot{\Gamma}^0_{11}\overline{\mathrm{A}}^{0\Gamma}\right\} d\Gamma^0_{11} \tag{4.17}$$

where Λ describes the coupling between the solid strain and the extent of reaction, consistent with the developments of [1]; λ^s, α^s, $\mu_L{}^s$, $\mu_T{}^s$, β^s are the transversely isotropic material constants, which in one dimension reduce to the elastic moduli of the solid. $\rho_T{}^s$, ρ_T are the true solid density and the true mixture density respectively. $\overline{R}$ is the ratio of the universal gas constant to the molecular weight of the fluid. $K_1^0 = -\rho\overline{K}_1$ and $A^{0\Gamma} = -\rho\overline{A}^{0\Gamma}$ are defined for convenient manipulations involving Λ.

Remark For the case of slurry deposition process that is presented in Sect. 4.3.2, Γ_{11}^0 represents the extent of material deposition. For this case, the term Λ provides coupling between the solid strain and the extent of deposition of the suspended particles. We assume that this deposition function Γ_{11}^0 is in fact a function of the volume fraction of particles, which is considered a process parameter.

4.1.1 Modeling Assumptions and Methodology

In mixture theory where both solid and fluid co-occupy the domain and fluid moves relative to the deforming solid, it is natural to write the fluid balance laws in an Arbitrary Lagrangian Eulerian (ALE) framework [2–4]. For the class of problems considered in this work, the inertial effects on the solid are assumed to be negligible.

Remark In [1] an expression for the rate of mass conversion for fluid m^f is derived via maximization of the rate of dissipation constraint. However, in the present work we prescribe an oxidation rate given in [5] that is developed based on physical measurements. Likewise, in the slurry infiltration model we prescribe a rate of particle deposition as is given in [6]. Because of these postulated rates, the physics involved in the consistent derivation of mass conversion given in [1] is circumvented. Thus,

$$m^f = \dot{\Gamma}_{11}^0 \tag{4.18}$$

4.2 Weak Form and Development of Stabilized Method

Let g^α and ${w_1}^\alpha$ denote the weighting functions for the balance of mass and linear momentum for the corresponding constituent, respectively.

4.2.1 Weak Form of Equations for the Fluid

$$\left(g^f, \left.\frac{\partial \rho^f}{\partial t}\right|_Y\right) + \left(g^f, \left(v_1^f - v_1^s\right)\frac{\partial \rho^f}{\partial x}\right) + \left(g^f, \rho^f \frac{\partial v_1^f}{\partial x}\right) - \left(g^f, m^f\right) = 0 \tag{4.19}$$

$$\left(\frac{\partial w_1^f}{\partial x}, T_{11}^f\right) - \left(w_1^f, \rho^f b_1\right) - \left(w_1^f, I_1^f\right) + \left(w_1^f, \rho^f \left.\frac{\partial v_1^f}{\partial t}\right|_Y\right) + \left(w_1^f, \rho^f \left(v_1^f - v_1^s\right)\frac{\partial v_1^f}{\partial x}\right) - \left(w_1^f, T_{11}^f n_1\right)_{\partial\Omega_h^f} = 0 \tag{4.20}$$

4.2.2 Weak Form of Equations for the Solid

$$\left(g^s, \frac{\partial \rho^s}{\partial t}\right) + \left(g^s, \rho^s \frac{\partial v_1^s}{\partial x}\right) + \left(g^s, v_1^s \frac{\partial \rho^s}{\partial x}\right) - \left(g^s, m^s\right) = 0 \tag{4.21}$$

$$\left(\frac{\partial w_1^s}{\partial x}, T_{11}^s\right) - \left(w_1^s, \rho^s b_1\right) - \left(w_1^s, I_1^s\right) - \left(w_1^s, T_{11}^s n_1\right)_{\partial\Omega_h^s} = 0 \tag{4.22}$$

where, $(\bullet,\bullet)=\int_{\Omega}(\bullet)\mathrm{d}\Omega$ is the $L_2(\Omega)$ inner product, $\left.\frac{\partial(\cdot)}{\partial t}\right|_Y$ represents the time derivative in the ALE frame [3, 4] and ${v_1}^m$ is the fluid mesh velocity. It is important to note that as the solid domain deforms, the Lagrangian mesh that is tied to material points deforms together with it. Consequently, the mesh velocity v_1^m is set equal to v_1^s where, v_1^s is the velocity of the solid domain.

4.2.3 Fluid Sub-system: Residual-Based Stabilization

Our objective is to model the diffusion of a chemically reacting fluid through a nonlinear elastic solid, a phenomenon that is observed in the process modeling of composites, oxidation of resin/composites, and slurry infiltration in porous media, to name a few. In the modeling of these processes, fluid mass concentration is invariably specified at the inlet boundary. Since the strong form of mass balance of fluid given in Eq. (4.1) is a first order hyperbolic equation, any specified mass concentration boundary condition at the inlet that is different from the initial condition results in a discontinuous fluid concentration field. This discontinuity introduces spurious oscillations in the computed solution right at the beginning of the nonlinear iterative process that can lead to non-convergent and therefore non-physical solutions.

To address this issue, we consider the weak form of the balance of mass equation for the fluid that is written in an ALE form. We employ Variational Multiscale (VMS) ideas [7–10] and develop a stabilized weak form for Eq. (4.19). Underlying idea of VMS is an additive decomposition of the solution field into coarse and fine scale components as given below.

$$\rho^f = \hat{\rho}^f + \widetilde{\rho}^f \tag{4.23}$$

$$g^f = \hat{g}^f + \widetilde{g}^f \tag{4.24}$$

where, $\hat{\rho}^f, \widetilde{\rho}^f$ represents the coarse-scale and fine-scale components of the density field and $\hat{g}^f, \widetilde{g}^f$ represents the coarse-scale and fine-scale counterpart of the weighting function respectively.

Substituting Eqs. (4.23) and (4.24) in Eq. (4.19) and employing the linearity of the weighting function slot in Eq. (4.19), we obtain the coarse-scale problem and the fine-scale problem as given in Eqs. (4.25) and (4.26) respectively.

$$\hat{W}^{\rho^f} = \left(\hat{g}^f, \left.\frac{\partial\left(\hat{\rho}^f + \widetilde{\rho}^f\right)}{\partial t}\right|_Y\right) + \left(\hat{g}^f, \frac{\partial\left(\hat{\rho}^f + \widetilde{\rho}^f\right)v_1^f}{\partial x}\right) - \left(\hat{g}^f, v_1^s \frac{\partial\left(\hat{\rho}^f + \widetilde{\rho}^f\right)}{\partial x}\right) - \left(\hat{g}^f, m^f\right) = 0 \tag{4.25}$$

$$\widetilde{W}^{\rho^f} = \left(\widetilde{g}^f, \left.\frac{\partial\left(\hat{\rho}^f + \widetilde{\rho}^f\right)}{\partial t}\right|_Y\right) + \left(\widetilde{g}^f, \frac{\partial\left(\hat{\rho}^f + \widetilde{\rho}^f\right)v_1^f}{\partial x}\right) - \left(\widetilde{g}^f, v_1^s \frac{\partial\left(\hat{\rho}^f + \widetilde{\rho}^f\right)}{\partial x}\right) - \left(\widetilde{g}^f, m^f\right) = 0 \tag{4.26}$$

It is important to note that both systems are nonlinear, and are also fully coupled in terms of the scales. The key idea at this point is to solve the fine-scale problem Eq. (4.26) locally, using analytical methods or numerical methods, and extract the fine-scale component, $\widetilde{\rho}^f$. This can then be substituted in the corresponding coarse-scale problem given in Eq. (4.25), thereby eliminating the fine-scales, yet modeling their effects.

4.2.4 Solution of the Fine Scale Problem

We segregate the terms into coarse-scale and fine-scale terms and group all the terms containing coarse-scale density field.

$$\widetilde{W}^{\rho^f} = \left(\widetilde{g}^f, \left.\frac{\partial\widetilde{\rho}^f}{\partial t}\right|_Y\right) + \left(\widetilde{g}^f, \frac{\partial\widetilde{\rho}^f v_1^f}{\partial x}\right) - \left(\widetilde{g}^f, v_1^s \frac{\partial\widetilde{\rho}^f}{\partial x}\right) + \left(\widetilde{g}^f, \hat{R}\right) = 0 \tag{4.27}$$

where, $\hat{R}$ is the residual of the Euler–Lagrange equations of the coarse-scales over element interiors and is given as,

$$\hat{R} = \left.\frac{\partial \hat{\rho}^f}{\partial t}\right|_Y + \frac{\partial \hat{\rho}^f v_1^f}{\partial x} - v_1^s \frac{\partial \hat{\rho}^f}{\partial x} - m^f\left(\hat{\rho}^f\right) \tag{4.28}$$

In obtaining the above form of the fine scale problem, we have assumed that the fluid mass conversion rate is a function of the coarse-scale fluid density field only, $m^f\left(\hat{\rho}^f, \widetilde{\rho}^f\right) \approx m^f\left(\hat{\rho}^f\right)$. Discretizing (4.27) in time and space results in a solution for the fine scale density field in terms of the coarse scale fields, expressed as a multiple of the residual. This solution confers stabilization properties resulting in the dampening of the oscillatory effects resulting from the boundary discontinuity. Details are given in [11].

4.3 Numerical Results

We present three test cases that investigate the stability and accuracy of the numerical method developed for the mixture theory model described in Sect. 4.3. The present developments have been carried out in the context of 1D finite element method, and extension to 3D case will be pursued in a subsequent paper.

4.3.1 Fick's Diffusion Problem

In this section we employ a reduced mixture model to solve Fick's diffusion problem. The transient Fick's diffusion equation can be derived from the mixture theory balance laws, Eqs. (4.1) and (4.2) based on the following simplifications: (a) solid is assumed to be rigid, (b) fluid is assumed ideal, (c) fluid inertial effects are neglected, and (d) fluid is assumed non-reactive.

Remark Solving for fluid velocity from the equation of motion and substituting into the equation of conservation of mass for the fluid, one can obtain Fick's diffusion equation. Since our full mixture model results in a first order system, in this work we have opted to solve the reduced system also in its first order form to help serve as a test case for evaluating our numerical method.

The unknown fields in this problem are the fluid concentration and fluid velocity that are solved with zero initial conditions. The one-dimensional domain of length 0.001 m is exposed to air at the left end of the domain where fluid concentration is assigned a value of 22.8863E−3 kg/m^3 and fluid velocity is constrained to be zero at the right end of the domain. The gas constant $\overline{R}$ and drag coefficient A^v are assigned values of 286.987 J/kg-K and 1.63E17 s^{-1}, respectively. We employ the Backward Euler scheme for time integration and run the problem for a total time of 30,000 s. A variable time step increment is used: the time steps employed during the first second is $\Delta t = 1\text{E} - 4$, and it is increased to $\Delta t = 0.1$ for the remaining steps.

It should be noted that the fluid mass balance equation is a first order hyperbolic equation for fluid concentration. For a non-zero fluid concentration boundary condition applied at the inflow, the standard Galerkin finite element method results in oscillations around the steep front thereby causing numerical instability. We employ the variational multiscale method to stabilize the formulation, and provide a comparison between the stabilized numerical result and the exact solution. Figure 4.1a, b shows performance of the new method for *h*-refinement wherein we have used linear Lagrange interpolation functions. These plots show the spatial profiles of the fluid concentration and velocity fields at 1,000, 10,000 and 30,000 s. It can be seen that as the number of elements is increased, computed solution converges to the exact solution which is a numerical validation of the consistency of the formulation. Improved convergence rate is obtained for quadratic elements, with similar stability properties.

4.3.2 Oxidation of PMR-15 Resin

Thermo-oxidative aging of polymer matrix composites (PMC's) in high temperature applications influences the life and performance of these materials. In this section, we present numerical results for the oxidation behavior of polyimide PMR-15 resin based on the oxidation reaction model developed in the works of Tandon et al. [5]. For the sake of completeness, we provide a brief description of the oxidation process in polymer. However, for a detailed description of the oxidation process and the reaction kinetics model, refer to [5, 12]. Oxidation front in polymer materials advances through a combination of diffusion and reaction mechanism. The exposed surface reacts with the diffusing air, depleting the amount of polymer

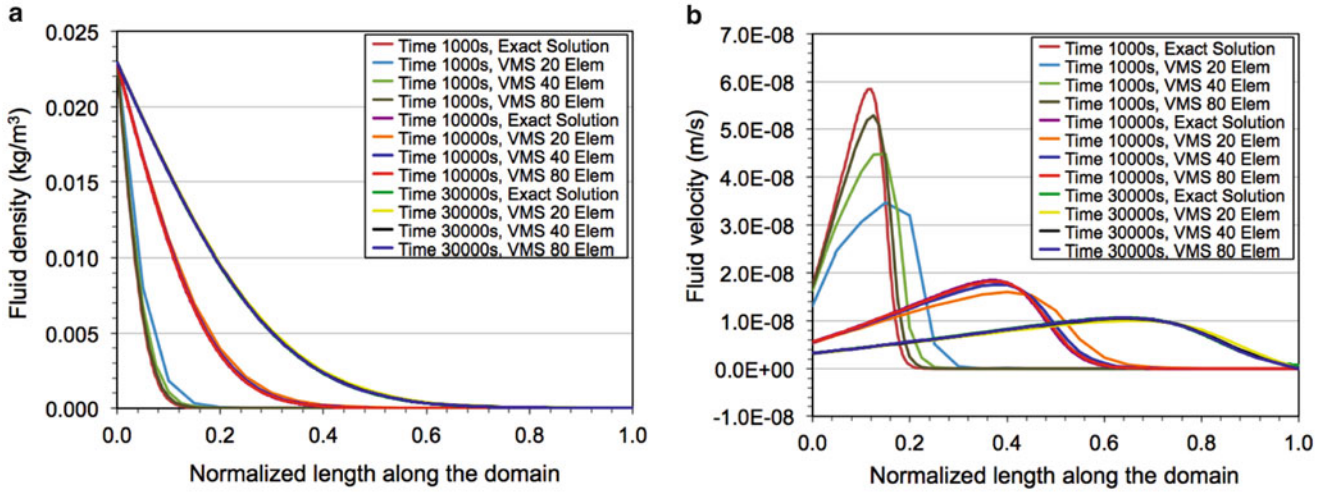

Fig. 4.1 Mesh refinement study at various time levels. (**a**) Fluid density: Linear Lagrange *h*-refinement. (**b**) Fluid velocity: Linear Lagrange *h*-refinement

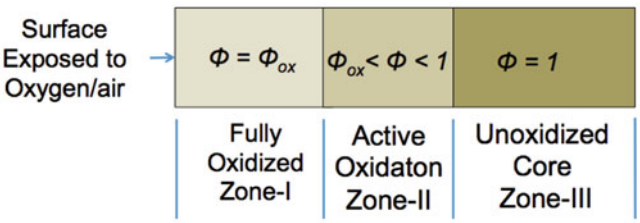

Fig. 4.2 Schematic representation of thermo-oxidation process

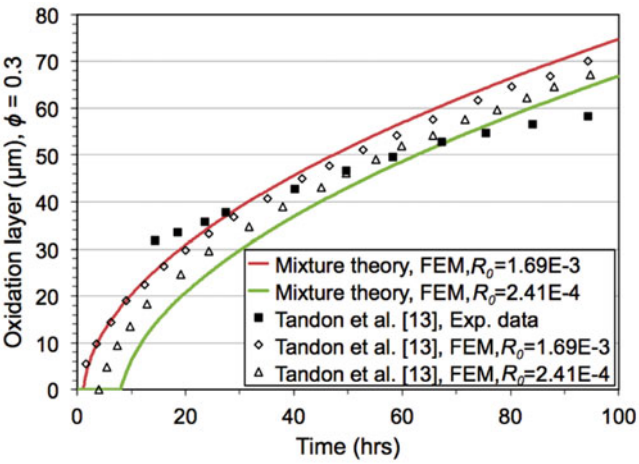

Fig. 4.3 Oxidation layer growth with time for various values of reaction rate

available to react in that region. Once this region is fully oxidized, it acts as a medium through which air/oxygen diffuses through and an active oxidation zone is formed ahead of the fully oxidized zone. Thus, at any instant of time, the oxidation process in polymers comprises of a fully oxidized zone, an active oxidation zone and a neat resin zone as shown in Fig. 4.2.

A parametric study was done for the oxidation layer growth with time and results are presented as shown in Fig. 4.3. The oxidation layer growth results shown in Fig. 4.3 are plotted for oxidative state parameter $\phi = 0.3$, a specific value within zone II [5, 12]. Figure 4.3 shows the variation in oxidation layer growth for different reaction rate parameters for a duration of 100 h. The solid line shows the results from the mixture theory, where it can be seen that the reaction rate of 2.41E−4 kg/m^3 s produces an oxidation layer growth of 66.9 μm as compared to 74.7 μm for the reaction rate of 1.69E−3 kg/m^3 s at the end of 100 h. The mixture theory results follow a similar trend in comparison with the Tandon et al. [5] numerical results.

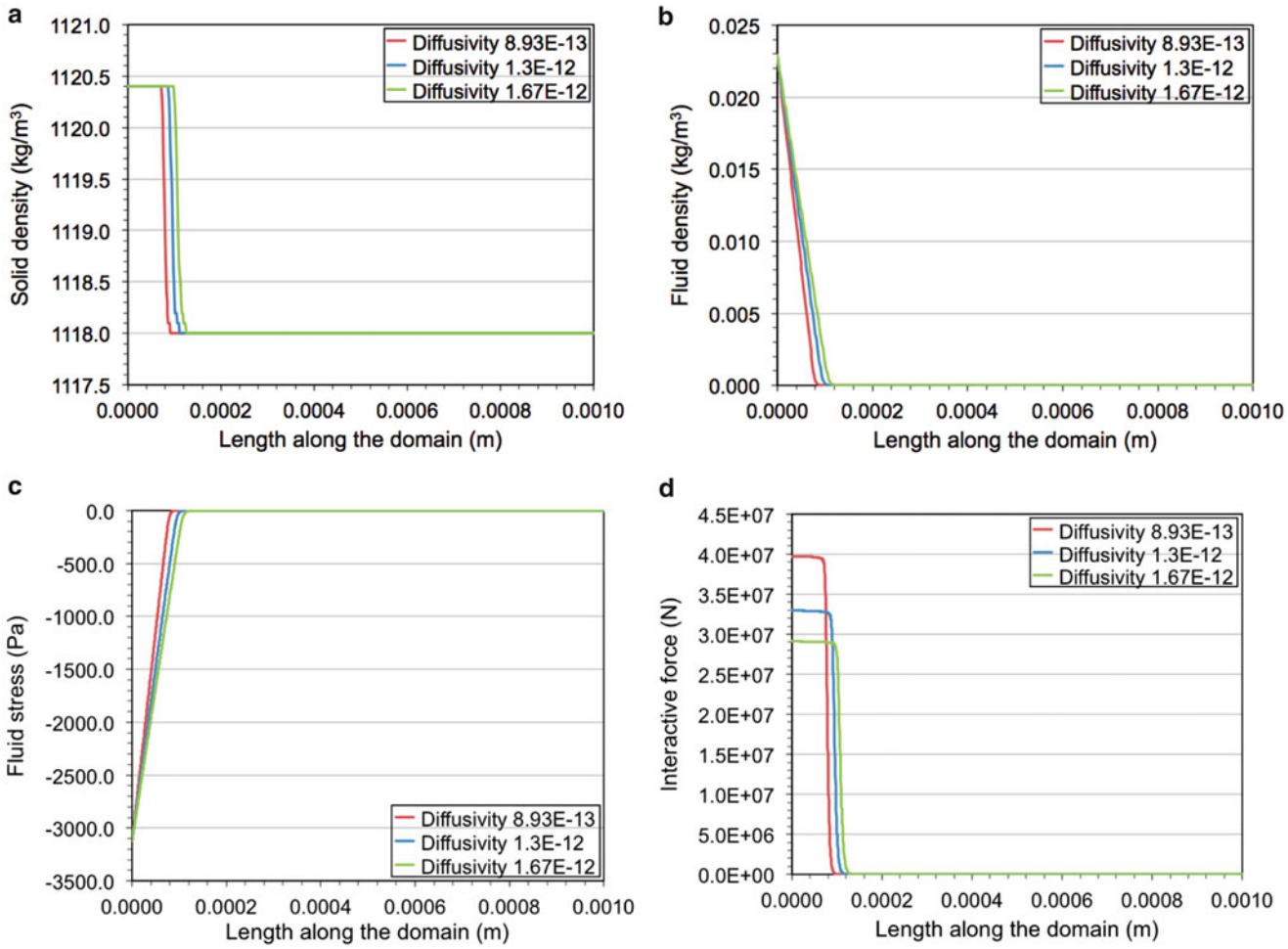

Fig. 4.4 Fluid and solid kinematic and force quantities along the domain at the end of 100 h. (**a**) Solid density along the domain, (**b**) fluid density along the domain, (**c**) fluid stress along the domain, (**d**) interactive force along the domain

Tandon et al. [5] studied the oxidation layer growth via diffusion reaction equation assuming an ideal fluid permeating through a rigid solid. Accordingly, in their model the deformation of the solid and viscous effects in the fluid are neglected. In the present work where we employ the mixture theory, a Newtonian fluid and an elastic solid are considered. The only additional assumed properties are two constants describing coupled chemomechanical and purely chemical dissipation, and standard values for viscosity of air and PMR-15 stiffness properties [11]. Since the unknown fields in the mixture model are fluid density, fluid velocity, solid displacement and solid density, therefore kinematic and the force measures can be readily obtained from the simulations. Figure 4.4 shows the variation of the fluid and the solid kinematic and force quantities for solid diffusivity values of 8.93E−13, 1.30E−12 and 1.67E−12 m^2/s. The plots shown are obtained for a saturated oxidation state value of $\phi_{ox} = 0.187$ and a reaction rate of 1.69E−3 kg/m^3 s. Figure 4.4a, b shows the variation of solid density and fluid density along the domain at the end of 100 h. Full oxidation of all presumed available sites results in a fixed solid density, as indicated in Fig. 4.4a.

Since there are only two constituents in the present model, loss of mass from one is the gain in mass for the other. Consequently, the density of the solid increases as shown in Fig. 4.4a wherein the apparent solid density has a higher value as compared to the neat resin region. This is rather contradictory to the experimental observations as the density of the PMR-15 resin is expected to decrease with increased levels of oxidation. (It does, however, correspond to initial weight gains in certain oxidizing materials systems before substantial mass loss to the environment occurs. The transfer of mass out of the material system is not explicitly addressed here.) If the two-constituent mixture model is extended to three-constituent model where the third constituent is allowed to evolve and also leave the domain, it can account for the experimentally observed weight loss in solid due to the oxidation process. Figure 4.4c shows that the variation in fluid stress is dominated by the hydrostatic pressure. Figure 4.4d shows the distribution of interactive force between the diffusing fluid and deforming solid. It can be seen that the interactive force becomes zero in the neat resin region where the fluid has not reached yet.

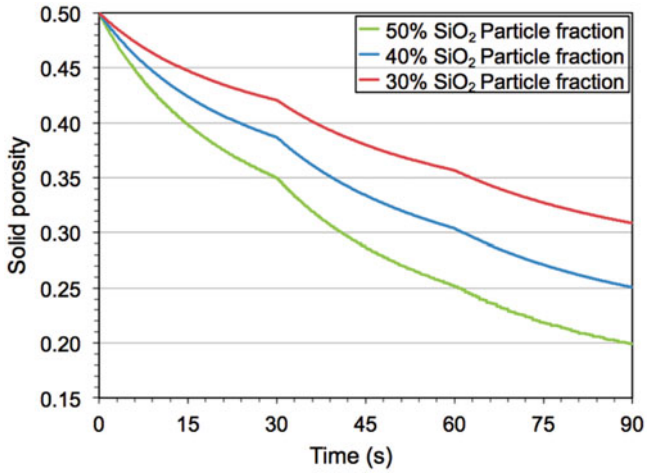

Fig. 4.5 Reduction in solid porosity with time for 30, 40 and 50 % SiO_2 particles in the slurry

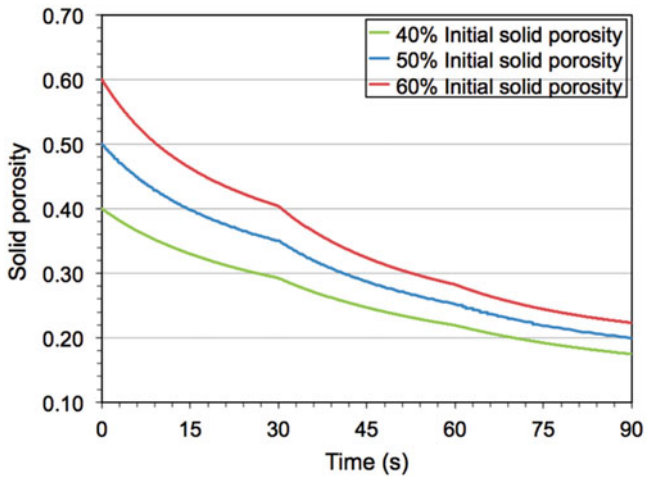

Fig. 4.6 Reduction in solid porosity with time for 40, 50 and 60 % initial solid porosity

4.3.3 Slurry Infiltration Problem

Slurry infiltration (SI) is an important step in the processing of ceramic matrix composites (CMC). In the slurry infiltration process, a viscous fluid that is laden with particles of various sizes, composition, and volume fraction is injected into a fiber preform, wherein fluid primarily serves as a medium that carries the suspended particles to the preform. This cycle is repeated several times till the density of the preform increases and its porosity reduces to some desired design value. Once slurry infiltration process is complete, a second process called melt infiltration is carried out with a viscous fluid that can chemically react with the preform as well as the deposited particles to make a composite with desired strength and density distribution [13].

In this section, we consider the SI and employ properties of a porous PMC as a surrogate model for CMC material. We assume that water based slurry has permeated the porous elastic solid and we model the process of deposition of suspension onto the fiber preform.

Below, we present the results for the case where the porous solid is subjected to three infiltration cycles of 30 s each, for a total of 90 s. At the end of each cycle, the particle mass fraction w is reset to the initial particle mass fraction in the slurry w_0. Figure 4.5 shows the variation of the solid porosity with time for 50 % porous solid and 30, 40 and 50 % SiO_2 particle volume fraction in the slurry. We see that as the particles get deposited, the porosity of the solid decreases. For all three different particle volume fractions in the slurry, this decrease in porosity is nonlinear, wherein the rate of reduction in porosity seems to be slowing down with time that is indicated by the relatively flatter portion of the curve at the end of each cycle. From the perspective of the physics of the problem this means that while there is more relative reduction in porosity during early infiltration cycles, because of the closure of pores that happens due to the solid mass buildup, the relative reduction in porosity in subsequent cycles also slows down. Figure 4.6 shows a similar trend in reduction in porosity with time for three different initial solid porosities that are infiltrated with 50 % particle slurry.

References

1. Hall R, Rajagopal K (2012) Diffusion of a fluid through an anisotropically chemically reacting thermoelastic body within the context of mixture theory. Math Mech Solids 17(2):131–164
2. Hughes TJ, Liu WK, Zimmermann TK (1981) Lagrangian–Eulerian finite element formulation for incompressible viscous flows. Comput Methods Appl Mech Eng 29(3):329–349
3. Khurram RA, Masud A (2006) A multiscale/stabilized formulation of the incompressible Navier–Stokes equations for moving boundary flows and fluid–structure interaction. Comput Mech 38(4–5):403–416
4. Calderer R, Masud A (2010) A multiscale stabilized ALE formulation for incompressible flows with moving boundaries. Comput Mech 46(1):185–197
5. Tandon G, Pochiraju K, Schoeppner G (2006) Modeling of oxidative development in PMR-15 resin. Polym Degrad Stab 91(8):1861–1869
6. Civan F (2011) Porous media transport phenomena. Wiley, Hoboken
7. Hughes TJR (1995) Multiscale phenomena: Green's functions, the Dirichlet-to-Neumann formulation, subgrid scale models, bubbles and the origins of stabilized methods. Comput Methods Appl Mech Eng 127(1):387–401
8. Masud A, Hughes TJR (1997) A space-time Galerkin/least-squares finite element formulation of the Navier–Stokes equations for moving domain problems. Comput Methods Appl Mech Eng 146(1):91–126
9. Masud A, Khurram R (2004) A multiscale/stabilized finite element method for the advection–diffusion equation. Comput Methods Appl Mech Eng 193(21):1997–2018
10. Masud A, Kwack J (2008) A stabilized mixed finite element method for the first-order form of advection–diffusion equation. Int J Numer Methods Fluids 57(9):1321–1348
11. Hall R, Gajendran H, Masud A (2014) Diffusion of chemically reacting fluids through nonlinear elastic solids: mixture model and stabilized methods. Math Mech Solids (in press)
12. Schoeppner G, Tandon G, Pochiraju K (2008) Predicting thermooxidative degradation and performance of high-temperature polymer matrix composites. In: Talreja R (ed) Multiscale modeling and simulation of composite materials and structures. Springer, New York, pp 359–462
13. Bansal NP, Boccaccini AR (2012) Ceramics and composites processing methods. Wiley.com, Hoboken